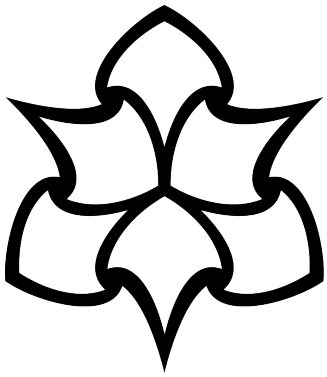

Titanium silicalite-1 macrostructures for photocatalytic removal of organic pollutants from aqueous media

S. P. D. Ormond[a], M. Ratova[a], P. Kelly[a], M. Edge[a], B. Mihailova[b], L. Tosheva[*,a]

[a] Faculty of Science and Engineering, Manchester Metropolitan University, Chester Street, Manchester, M1 5GD, United Kingdom

[b] Mineralogisch-Petrographisches Institut, Universität Hamburg, Grindelallee 48, D-20146 Hamburg, Germany

Abstract

Titanium silicalite-1 (TS-1) structures in the form of macroscopic beads with hierarchical porosity were prepared by the resin templating method. The Ti content within the samples was varied between 1 and 7 wt.%, with corresponding surface areas ranging from 725 to 350 $m^2 g^{-1}$, respectively. The samples contained a large amount of amorphous material, which was necessary to achieve high mechanical stability of the beads. The TS-1 macrostructures were used as catalysts for the photocatalytic degradation of methylene blue (MB), and results were compared to the results for a commercial anatase nanopowder (CristalACTiV™ PC500). All TS-1 beads showed similar MB degradation rates independently of their Ti content, which was linked to variations in the surface areas and structure. The macroscopic shape of the TS-1 beads allowed easy recovery from the mother liquor upon decolouration of the MB solutions, which was highly beneficial compared to the reference anatase nanopowder. The TS-1 beads could be reused in subsequent photocatalytic cycles after decanting exhausted solutions and replacing with fresh MB solutions without any energy-consuming

[*]Corresponding author. Tel.: +44 161 274 1426; Fax: +44 161 274 6840

E-mail address: l.tosheva@mmu.ac.uk (L. Tosheva)

regeneration steps involved. The samples were tested in five consecutive cycles and MB degradation rates remained broadly unchanged during all tests.

1. Introduction

Heterogeneous catalysis plays a central role in modern life for the production of fuels, pharmaceuticals, agricultural and other chemical products and for environmental protection. The continuous development of novel solid catalysts with an impact on energy consumption, either during synthesis or during operation and post-treatment, is of paramount importance for the urgently needed transition to a low-carbon world. The synthesis of titanium silicalite-1 (TS-1), an MFI-type zeolite containing titanium atoms in silicon substitutional framework positions, was firstly reported in 1983 by Taramasso *et al.* [1]. The unique catalytic properties of TS-1 have generally been associated with the presence of isolated tetrahedral Ti atoms within silicalite-1 [2,3]. The nature of Ti species in TS-1 has been extensively studied and different framework and non-framework Ti species have been identified by a number of advanced characterization techniques [4-7]. Owing to its high selectivity and activity in oxidation reactions with H_2O_2 under mild conditions [8], there have been continuous efforts to develop TS-1 materials with improved properties for specific catalytic reactions. Introduction of mesoporosity has been explored to overcome diffusion limitations imposed by the medium pore size of TS-1. Serrano and co-workers have prepared hierarchical TS-1 zeolites with enhanced catalytic activity from silanized protozeolitic units [9], which mesopore size distribution could be further narrowed by a post-synthesis treatment with cationic surfactants [10]. Hierarchical TS-1 zeolites with improved catalytic properties have been synthesized using hard templates such as carbon or by recrystallization of prefabricated TS-1 nanoparticles [11,12]. A remarkable enhancement of the catalytic activity of TS-1 in oxidative desulfurization has been achieved by creating mesoporosity through post-synthesis chemical etching in the presence of NH4F-HF

[13]. A drawback in the above examples is the powder form of the hierarchical TS-1 materials, which makes them difficult to separate from mother liquors, particularly if nanosized crystals are employed. Thus, a step further would be the preparation of hierarchical TS-1 materials, which are easily recoverable. For example, such materials have been synthesized through hydrophobicity control, crystallisation in a quasi-solid-state system or with the aid of triblock copolymers [14-16].

Green water treatment technologies to remove dyes and other organic pollutants from industrial effluents have become of increasing importance in recent years. Processes based on adsorption and biological treatments are inefficient due to accumulation of waste and recyclability costs [17,18]. Photocatalytic dye degradation in the presence of TiO_2 semiconductor catalysts has provided a sustainable and environmental friendly alternative [19-21]. Advantages include operation under ambient temperatures and pressures and complete mineralization of the dyes, however, aggregation of the TiO_2 nanoparticles typically used in the process and difficulties in their post-separation are obstacles that limit the process efficiency. The preparation of structured 700 nm TiO_2 beads with permanent mesoporosity has been reported [22]. These materials showed similar photocatalytic activity to a commercial P25 photocatalyst, however their size was still not large enough to allow for an instant separation from the mother liquor.

TS-1 has been used as photocatalyst for degradation of organic molecules such as monoethanolamine and 4-nitrophenol in the presence or absence of H_2O_2 [23,24]. Its photocatalytic activity per weight of catalyst was found to be lower compared to that of TiO_2, however its intrinsic activity per Ti atom was higher as a result of its zeolitic

structure [23]. The TS-1 photocatalytic activity could be further increased by hybridizing TS-1 with graphene [25].

Despite the potential of TS-1 materials in photocatalytic water cleaning technologies, the use of macroscopic TS-1 structures with hierarchical porosity has not been largely explored. We have used the resin templating method to prepare different types of zeolites in the form of macroscopic, > 0.1 mm, self-bonded beads with secondary mesoposity [26-28]. Titanosilicate beads with an amorphous structure and incipient TS-1 features or MCM-41-like disordered structure have also been prepared using ion-exchange resins as templates [29,30]. The materials showed enhanced catalytic activity in the epoxidation of cyclohexane compared to conventional TS-1, which was ascribed to their hierarchical porosity. In addition, the materials were immune to Ti leaching and easy to recycle. Macroscopic TiO_2-SiO_2 porous beads were also prepared by resin templating and tested as photocatalysts [31]. The materials were amorphous when the TiO_2 fraction was less than 40%, and anatase was detected in XRD patterns upon increasing the TiO_2 content above that level. These works clearly demonstrate the advantages of the macroscopic shape and the resin-originating mesoporosity for the catalytic/photocatalytic properties of TiO_2 materials. In the present work, the resin templating method was used to prepare TS-1 macroscopic beads to evaluate the role of the TS-1 isolated tetrahedral titanium atoms for the photocatalytic activity of the materials. The photocatalytic activity was determined for the degradation of methylene blue as a model dye molecule.

2. Experimental

2.1. Synthesis of TS-1 macroscopic beads

TS-1 macrostructure synthesis was achieved through the use of a TS-1 clear synthesis solution with molar composition of 9TPAOH : $xTiO_2$: $25SiO_2$: $404H_2O$, where x= 0.25, 0.5 or 1.0 [32]. The synthesis solution was prepared by firstly mixing tetraethoxysilane (98%, Sigma-Aldrich) and titanium (IV) ethoxide (98%, Lancaster). Tetrapropylammonium hydroxide (TPAOH) (1M aqueous solution, Alfa Aesar), was then added dropwise at a rate of 1 ml min^{-1} in order to prevent the formation of anatase. Once all the TPAOH had been added, the TS-1 synthesis solution was left to hydrolyze for one hour, using vigorous stirring. Amberlite IRA-900, a strongly basic macroporous anion exchange resin (chloride form, Alfa Aesar) was mixed with the TS-1 synthesis solution at a solution to resin weight ratio of 10. The mixture was then transferred into PTFE-lined stainless steel autoclaves and hydrothermally treated using a two stage temperature synthesis [33]. After an initial treatment at 100 °C for 48 h, the temperature was increased to 170 °C and treatment continued for 6 h at the higher temperature. After the synthesis, the resin-TS-1 beads were separated from the mother liquid by decanting, rinsed with distilled water and ultrasonicated to remove loose bulk phase material, and dried at 60 °C. Finally, the TPA and resin templates were removed by calcination at 600 °C for 10 h after heating to this temperature at a rate of 10 °C min^{-1}. The samples obtained were denoted as TS-1(0.25), TS-1(0.5) and TS-1(1.0), according to the different x used in the molar composition of the synthesis solution. A reference silicalite-1 (S-1) sample was also prepared for a comparison. The silicalite-1 sample was prepared as above from a synthesis with the molar composition of 9TPAOH :

$25SiO_2$: $480H_2O$ with a hydrothermal treatment at 100 °C for 17 h followed by treatment at 170 °C for 10 h [33].

2.2. Characterization methods

Scanning electron microscopy (SEM) was used to study the morphology of the TS-1 beads. SEM images were recorded with a Supra 40VP microscope from Carl Zeiss Ltd. The Ti content of the beads was determined by energy-dispersive X-ray (EDX) spectroscopy using an Apollo 40 SDD detector (EDAX Inc.). The average of five measurements was used on uncoated tablets prepared from carefully ground beads. X-ray diffraction (XRD) patterns of ground samples were obtained with an X'Pert PANalytical X-ray diffractometer employing Cu Kα radiation (40 kV and 30 mA) and a PIXcell detector. Nitrogen absorption measurements of calcined beads were performed at -196 °C with a Micromeritics ASAP 2020 surface area analyser. Samples were outgassed at 300 °C for 12 hours prior to analysis. Surface areas (S_{BET}) and pore size distributions were determined using the BET equation and BJH (desorption branch of the isotherm) method, respectively. Total pore volumes (V_{total}) were obtained from the volume adsorbed at a relative pressure of 0.99, whereas micropore volumes (V_μ) and external surface areas (S_{EXT}) were determined from t-plot analysis. Raman-scattering experiments were performed on S-1 and TS-1 zeolite beads and CristalACTiV™ PC500 with a Horiba Jobin-Yvon T64000 triple-monochromator spectrometer equipped with a LN_2-cooled Symphony CCD detector and an Olympus BH41 microscope with a 50x long-working distance objective. Spectra in the range 15 - 4000 cm^{-1} were collected in backscattering geometry using the 514.5 nm line of an Ar^+-ion laser (Coherent Innova 90C FreD). The laser power on the sample surface was 5.9 mW, while the diameter of the laser spot on the sample surface was approximately 2 μm. No polarization,

orientation, or spatial dependence of the Raman spectra was detected, indicating that the average linear crystallite size is much smaller than linear size of the probed sample volume. The achieved spectral resolution was 1.9 cm^{-1}, while the precision in the peak positions was 0.35 cm^{-1}. Measurements with lower laser powder verified the absence of undesired sample overheating while collecting spectra. Additional experiments with an excitation wavelength of 488.0 nm proved that all observed peaks originate from atomic vibrations rather than from photoluminescence. The measured spectra were baseline corrected for the continuum photoluminescence background and temperature-reduced to account for the Bose-Einstein occupation factor. Microwave resonance broadband dielectric loss (BDS) measurements with simultaneous UV irradiation were undertaken using a Marconi (6200A) 2-20 GHz programmable sweep generator and automatic amplitude analyser, coupled to a rectangular waveguide and cylindrical cavity. CristalACTiV™ PC500 and TS-1(0.25) samples (0.2 g) placed in the cavity were irradiated in the cell chamber with an ILC 302UV xenon source (Laser Lines Ltd.) via an optical fibre and data corrected for sample density. Attenuation of the power stored by the microwave cavity (± 0.05 dBm) was monitored at 25 °C in real-time during 1800 s of irradiation and then for a further 1800 s with the light-source switched-off.

2.3. Photocatalytic tests

Stock solutions of methylene blue (MB) (BDH Chemicals) with concentrations of 0.03 - 0.2 mM were prepared and used within one week of preparation; all stock solutions were kept in the dark. CristalACTiV™ PC500 (100% anatase, BET surface area of 345 $m^2 g^{-1}$, particle size of 5-10 nm) was used as a commercial TiO_2 reference material. In a typical photocatalytic run, MB solutions (10 mL) with an appropriate concentration were added to 0.2 g of TS-1 or reference materials in closed glass vials

covered with foil. The vials were transferred to an orbital incubator (Stuart Scientific) at 35 °C and kept for 3 h at 100 Rev min^{-1} to eliminate adsorption effects from subsequent MB degradation rates determinations.

After conditioning the samples for 3 h to account for adsorption, the samples (cap- and foil-free vials) were placed in an Atlas Suntest CPS+ cabinet (1500 W xenon lamp, 400 W m^{-2} irradiance) and irradiated in 15 min doses at 35 °C. After each dose, the vials were removed from the cabinet and aliquots of dye were removed for UV-Vis analysis. In the case of CristalACTiV™ PC500, six different vials were prepared initially and individual samples were used for each measurement after centrifugation (MSE Mistral 2000 centrifuge, 4500 rpm, 5 min) to separate the CristalACTiV™ PC500 from the mother liquor. Owing to the small particle size of CristalACTiV™ PC500, it was not possible to use the same sample in the measurements due to material loss during centrifugation. UV-Vis measurements were performed with an Agilent Cary 8454 UV-Vis spectrophotometer. Pseudo-first order kinetics of the degradation of MB was applied to calculate apparent rate constants using absorbance data at 665 nm. After the UV-vis measurements, the dye aliquots were returned to the vials and samples were irradiated with the next 15-min dose. Vials were equilibrated at 35 °C prior to returning to the Suntest cabinet. Initial MB concentrations were adjusted during preliminary adsorption experiments so that the dye concentration after adsorption was about 0.03 mM for all samples. MB solution in the absence of a catalyst was measured under the same conditions as well.

To determine the reusability of TS-1 samples, the decoloured MB solutions were decanted and replaced with fresh MB solutions without any washing or other laboratory procedures involved. The photocatalytic tests were repeated four more times.

Experiments were also performed after regenerating the beads by calcination at 600 °C for 10 h between runs.

3. Results and discussion

TS-1 beads were firstly prepared by a single stage hydrothermal treatment at 100 °C or 170 °C. Similarly to our previous results for silicalite-1, the samples prepared by direct synthesis at 100 °C contained a large amount of amorphous material (Supporting Information, Fig. S1) [26]. The single treatment at 170 °C yielded a highly crystalline material, however the beads were hollow and fragile (Supporting Information, Fig. S2). Such hollow spheres have been obtained previously during the synthesis of ZSM-5 by resin templating [28]. Thus, a two stage temperature synthesis was employed to increase the TS-1 crystallinity compared to samples prepared at 100 °C with preservation of their high mechanical strength [33]. The treatment time at 100 °C was fixed at 48 h and the treatment time at 170 °C was varied between 6 and 12 h. The mechanical stability increased by decreasing the treatment time at 170 °C, which was accompanied with a decrease in crystallinity (not shown). Samples prepared for 7 h were still brittle; therefore a treatment time of 6 h was selected for the samples used in this study. XRD patterns of the corresponding TS-1 samples are shown in Fig. 1. The results indicate that all Ti-containing samples are composed of a crystalline phase of MFI-type zeolite and a large amount of amorphous material. The latter conclusion was drawn by the presence of an amorphous halo between 15 and 35 ° 2θ in the XRD patterns of TS-1 beads (Fig. S3). The TS-1 crystallinity decreased with the increase in the Ti content from TS-1(0.25) to TS-1(1.0) as judged by the decrease in the intensity of the MFI-type peaks (Fig. 1).

The TS-1 beads were similar in size and shape to the resin beads used as templates (Fig. 2). A small number of cracked particles was present in samples TS-1(0.25) and TS-1(0.5), whereas this number was larger in TS-1(1.0) (Fig. 1c-d). Nevertheless, qualitative inspection during grinding indicated that all TS-1 samples showed high mechanical stability independently of the Ti content. The interior of the beads was built from fine nanoparticles and all samples were similar, independent of their Ti content (Supporting Information, Fig. S4). This has been observed for all zeolites prepared by the resin templating method and explained by the confined resin space available for the zeolite crystallisation: crystal growth is limited by the resin polymer chains to the size of the resin macropores, which is about 100 nm [26-28]. There are no limitations for crystal growth on the surface and larger crystals with a typical MFI morphology can be observed on the surface of TS-1 beads (Fig. 3). The surfaces of the TS-1(0.25) and TS-1(0.5) were similar in appearance (Fig. 3a and b). There were two distinct surface morphologies for sample TS-1(1.0) (Fig. 3c,d), indicating that this sample is less homogeneous compared to the other two and that an additional phase may be present in this sample.

The nitrogen adsorption isotherms of the TS-1 beads are shown in Fig. 4a. The isotherms contain mesopores as evident from the hysteresis loop at high relative pressures, as well as micropores as indicted by the steep increase in the volume adsorbed at low relative pressures. The mesopores had pore size distributions in the range 20-50 nm (Fig. 4b). No substantial differences in the secondary porosity of the three samples could be detected, which is not surprising considering that the secondary porosity is formed during resin removal. The gas adsorption data included in Table 1 indicate that there are variations in the BET surface areas, external surface areas, micro

and mesopore volumes between the samples, which are most pronounced for TS-1(1.0). In particular, the unusually high external surface areas of TS-1(0.25) and TS-1(0.5) could be related to the presence of a high surface area amorphous material. The external surface area of TS-1(1.0) drastically decreases, which suggests the formation of a dense phase, which is in agreement with the SEM results for that sample (Fig. 3c,d). The Ti content determined by EDX is provided in Table 1. It has been reported that the highest Ti content incorporated into the MFI structure was 2.5 Ti atoms / unit cell (2.8 mol-% Ti) [1], although the synthesis of TS-1 with a higher Ti content of up to 4.0 mol% has also been described [34]. Thus, whereas the large decrease in the surface area of TS-1(1.0) clearly indicates the presence of non-framework Ti, the high Ti content measured for TS-1(0.5) means that the presence of impurities of non-framework Ti in this sample is very likely. The increase in the mesopore volume and the external surface area for that sample, which is accompanied with a decrease in the micropore volume supports the possible presence of impurities of amorphous Si-Ti phases in TS-1(0.5).

Raman analysis was further used to determine the structure of the TS-1 beads as a method sensitive to the short- and intermediate-range structure (Fig. 5). Different spots on the spheres were measured and the spectra shown are representative of the samples, except for TS-1(1.0), for which two distinct types of spectra were measured, as shown in the figure. The most intense silicalite-1 peak at 380 cm^{-1} is present in all TS-1 samples. However, the Raman scattering near 495 cm^{-1} associated with the presence of amorphous silica is increasing with an increase in the Ti content in agreement with the XRD results [33]. The sharp Raman peak at 3750 cm^{-1} due to surface silanol groups decreases from TS-1(0.25) to TS-1(0.5) and is absent in TS-1(1.0). Since the relative intensity of this peak depends on the surface-to-bulk ratio, it is indicative of the

presence of small grains, which would explain the high external surface areas of these two samples. The band near 960 cm^{-1} has been used as a fingerprint of Ti incorporated into the MFI-type framework, i.e. it as a marker of TS-1 [3]; its intensity increases with an increase in the Ti content. A slight shift of this band towards lower wavenumbers was observed in some of the Raman spectra of TS-1(1.0), which can be associated with the presence of water [35], as detected by the broad Raman band between 3200 and 3600 cm^{-1}. In addition, the Raman peak at 150 cm^{-1} unambiguously indicates the presence of an anatase impurity phase in this sample, which is in agreement with SEM and gas adsorption results.

The TS-1 beads were studied as photocatalysts for the degradation of MB. The MB solutions retained their bluish colour in the presence of the reference S-1 beads indicating that the Ti-free beads were not photocatalytically active (Supporting Information, Fig. S5). Absorbance spectra of MB solutions before and after UV irradiation in the absence of photocatalysts and in the presence of CristalACTiV™ PC500 or TS-1 beads are shown in Fig. S6, Supporting Information. The absorbance peak centred at 665 nm in MB is due to the hetero-polyaromatic linkage. The 665 nm peak exhibits a shoulder at 615 nm, corresponding to monomers and dimers respectively [36]. Upon irradiation in the presence of CristalACTiV™ PC500, the peak at 665 nm shows a hypsochromic shift (blue shift to shorter wavelengths). This is caused by the N-demethylated degradation occurring concomitantly with the degradation of the phenothiazine functionality. Radicals from the photocatalyst, which is in direct coulombic interaction with the MB, cleave the bonds of the $C–S^{+}=C$ functional group to C–S(=O)–C. This in turn requires the conservation of the double bond conjugation, which induces the opening of the central aromatic ring containing both heteroatoms, S

and N. Such a shift was not observed in the case of catalyst-free MB solutions or MB solutions in the presence of TS-1 beads (Supporting Information, Fig. S6). The different results obtained for CristalACTiV™ PC500 and TS-1 may be attributed to agglomeration of the CristalACTiV™ PC500 fine particles in solution upon standing, whereas theTS-1 beads, with their highly porous structures, are free flowing.

Plots of $\ln(A/A_0)$, where A_0 is the absorbance at 665 nm after the 3-hours conditioning prior to UV irradiation and A is the corresponding absorbance at different irradiation times, against time were used to calculate the apparent first-order rate constants, k_{app} (Table 2). The results indicate that CristalACTiV™ PC500 was about 1.2 - 1.5 more active compared to TS-1 beads (Fig. 6). However, the TS-1 beads could be easily reused by simple decanting without an apparent loss of activity in at least five cycles.

The photocatalytic degradation mechanism of MB in the presence of TiO_2 has been discussed in detail before [37]. In this work, there were no substantial differences in the MB degradation rates for the TS-1 samples of different Ti content. XRD, gas adsorption and Raman results indicated that upon increasing the Ti content, TS-1 crystallinity decreases, surface area decreases and anatase is formed. It is well-known that anatase shows the highest photocatalytic activity of TiO_2 materials. Thus, it seems that the effect of the decreased surface area is compensated by the formation of anatase with preservation of the beads' mesoporous structure, resulting in a similar photocatalytic activities of the three TS-1 samples. Such an inverse trend in the influence of the amount of titanium and the surface area on the photocatalytic activity of TiO_2-SiO_2 beads prepared by resin templating has been suggested before [31]. Additionally, the presence of water in TS-1(1.0) detected by Raman spectroscopy (Fig.

5) suggests that the increased hydrophilicity of this sample may also have a negative influence on the diffusion of MB resulting in a reduced photocatalytic activity.

In reference [31], the conversion of MB over porous TiO_2-SiO_2 beads prepared by resin templating was markedly lower compared to a reference P25 TiO_2 catalyst, whereas the results for the conversion of phenol over these catalysts were comparable. This result was explained by diffusion limitations of the bulky dye molecule. Our previous results for materials prepared by resin templating [26-28], as well as the results reported here, indicate that the variations in the secondary porosity created by the resin removal are not great. In other words, the secondary porosity of the materials reported here is similar to the secondary porosity of the materials reported in reference [31]. Thus, the unique TS-1 active centres seem to be responsible for the comparable MB degradation rates obtained for TS-1 and CristalACTiV™ PC500 in our work, demonstrating the potential of hierarchical free flowing TS-1 materials for the photocatalytic degradation of bulky organic molecules.

It is interesting that TS-1 influences the rate of degradation of MB monomers and dimers to the same extent, whereas for CristalACTiV™ PC500 the rate of degradation of MB monomers is significantly higher than that for MB dimers (Supporting Information, Fig. S7). This may be due to the porosity in TS-1 facilitating accessibility and hence coulombic interactions. The different rates also suggest that the dye binding sites to CristalACTiV™ PC500 are weaker compared to the TS-1 ones, with the binding for the dimers being stronger.

The photocatalytic properties of CristalACTiV™ PC500 and TS-1 were further studied using BDS measurements (Fig. 7). Unlike time-resolved microwave conductivity measurements, which monitor decay of conductivity following a high

intensity pulse of radiation, the real-time method is able to probe excess charge carrier dynamics over extended periods, and correlate them with the surface reactions taking place. The creation of large numbers of phonons (heat) as mobile free carriers are generated reduces the ability of the microwave cavity to store power (attenuation of microwave power). Power is stored by the cavity at certain frequencies due to the oscillating electric and magnetic fields of the microwave energy that reach a maximum when they are resonant with the cavity. In effect, the separation of charge reduces the (imaginary part of the) dielectric constant and increases the conductivity of the material. Figure 7 indicates that the temporal profiles of CristalACTiV™ PC500 and TS-1 are distinctly different. The greater attenuation of power stored by the microwave cavity for CristalACTiV™ PC500 suggests that more free-carriers are produced in this high surface area nano-anatase. The power reached a maximum rapidly and thereafter levels-off as free-carrier production is in competition with shallow-trapping at surface sites and recombination of carriers. After 1800 s, the light source is switched off and a rapid decrease in attenuation of power is seen as free carriers recombine. For TS-1 the initial reduction in microwave power is not so pronounced as for CristalACTiV™ PC500 suggesting that either fewer free carriers are produced or that free carriers more effectively recombine and/or are trapped. Previous studies have shown that silica and alumina on the surface of TiO_2 can effectively trap free carriers [38]. Such trapping may be taking place in the zeolite silica framework or amorphous silica matrix, thereby reducing free carrier populations and so reducing photoactivity. However, there is a slower reduction of attenuated power in the case of TS-1 after switching off the source, suggesting that trapped carriers are recombining more slowly.

Although beyond the scope of this study, the qualitative analysis of the MB adsorption on S-1 and TS-1 beads showed that MB is strongly adsorbed and cannot be removed by UV irradiation (Supporting Information, Fig. S4); the intense bluish colour of the beads is retained between photocatalytic cycles. Consequently, the MB adsorption on the S-1 and TS-1 beads upon reuse is substantially reduced. The fact that the rate constants between cycles are similar indicates that the adsorbed MB is not blocking the active photocatalytic centres and does not influence the photocatalytic process. The original S-1 and TS-1 beads adsorption capacity could be restored after calcination at 600 °C. However, repeated regeneration by calcination lead to structural transformations such as formation of anatase as detected by Raman analysis (not shown).

Conclusions

Porous TS-1 beads with hierarchical microporous/mesoporous structure were prepared by the resin templating method. Three samples with Ti content of 1.1, 3.1 and 6.9 wt.%, respectively, were prepared. All samples contained a large amount of amorphous material, which fraction increased with an increase in the Ti content. The surface area of the sample containing 6.9 wt.% Ti drastically decreased due to the formation of anatase as determined by Raman analysis. The photocatalytic activity of the TS-1 beads was evaluated for the degradation of methylene blue, and compared to that of a commercial CristalACTiV™ PC500 TiO2. The activity of CristalACTiV™ PC500 was up to 1.5 times higher compared to TS-1. However, the macroscopic shape of the TS-1 beads facilitated their recycling and reuse in at least four additional cycles without any loss of material or regeneration steps involved. The TS-1 beads were separated from the mother liquor after each photocatalytic cycle by simple decanting

and fresh dye solutions were added. Further, the TS-1 samples of different Ti content showed similar activities, which was due to compensating surface area / Ti content and hydrophilicity effects on the activity. Microwave resonance broadband dielectric loss (BDS) measurements showed that more free carriers were produced by CristalACTiV™ PC500 compared to TS-1, which recombined more rapidly upon switching off the light source. Although the results show that the photoactivity of CristalACTiV™ PC500 is better than TS-1, the data presented suggest that the TS-1 samples could be further optimised to circumvent any free carriers trapping and so give comparable photoactivity to that of the CristalACTiV™ PC500, but with the added advantage of easier recycling and reuse in liquid media photocatalytic reactions.

References

[1] M. Taramasso, G. Perego, B. Notari, US Patent No 4410501 (1983)

[2] A. Tuel, J. Diab, P. Gelin, M. Dufaux, J.-F. Dutel, Y. Ben Taarit, J. Mol. Catal. **63**, 95-102 (1990)

[3] A. Zecchina, S. Bordiga, C. Lamberti, G. Ricchiardi, C. Lamberti, G. Richiardi, D. Scarano, G. Petrini, G. Leofanti, M. Mantegazza, Catal. Today **32**, 97-106 (1996)

[4] C. Lamberti, S. Bordiga, D. Arduino, A. Zecchina, J. Phys. Chem. B **102**, 6382-6390 (1998)

[5] J. Su, G. Xiong, J. Zhou, W. Liu, D. Zhou, G. Wang, X. Wang, H. Guo, J. Catal. **288**, 1-7 (2012)

[6] Q. Guo, K. Sun, Z. Feng, G. Li, M. Guo, F. Fan, C. Li, Chem. Eur. J. **18**, 13854-13860 (2012)

[7] C. Liu, J. Huang, D. Sun, Y. Zhou,X. Jing, M. Du, H. Wang, Q. Li, Appl. Catal. A **459**, 1-7 (2013)

[8] G. Bellussi, V. Fattore, Stud. Surf. Sci. Catal. **69**, 79-92 (1991)

[9] D. P. Serrano, R. Sanz, P. Pizarro, I. Moreno, S. Medina, Appl. Catal. B **146**, 35-42 (2014)

[10] D. P. Serrano, R. Sanz, P. Pizarro, I. Moreno, S. Shami, Micropor. Mesopor. Mater. **189**, 71-82 (2014)

[11] H. Xin, J. Zhao, S. Xu, J. Li, W. Zhang, X. Guo, E. J. M. Hensen, Q. Yang, C. Li, J. Phys. Chem. C **114**, 6553-6559 (2010)

[12] Y. Xue, Y. Wen, H. Wei, M. Liu, X. Huang, X. Ye, X. Wang, B. Li, RSC Adv. **5**, 51563-51569 (2015)

[13] S. Du, X. Chen, Q. Sun, N. Wang, M. Jia, V. Valtchev, J. Yu, Chem. Commun. **52**, 3580-3583 (2016).

[14] Q. Lv, G. Li, H. Sun, Fuel **130**, 70-75 (2014)

[15] L.-H. Chen, X.-Y. Li, G. Tian, Y. Li, J. C. Rooke, G.-S. Zhu, S.-L. Qiu, X.-Y. Yang, B.-L. Su, Angew. Chem. Int. Ed. **50**, 11156-11161 (2011)

[16] Z. Wang, L. Xu, J. Jiang, Y. Liu, M. He, P. Wu, Micropor. Mesopor. Mater. **156**, 106-114 (2012)

[17] T. Robinson, G. McMullan, R. Marchant, P. Nigam, Bioresource Technol. **77**, 247-255 (2001)

[18] G. Crinin, Bioresource Technol. **97**, 1061-1085 (2006)

[19] I. K. Konstantinou, T. A. Albanis, Appl. Catal. B **49**, 1-14 (2004)

[20] M. N. Chong, B. Jin, C. W. K. Chow, C. Saint, Water Res. **44**, 2997-3027 (2010)

[21] A. Ajmal, I. Majeed, R. N. Malik, H. Idriss, M. A. Nadeem, RSC Adv. **4**, 37003-37026 (2014)

[22] X. Wang, L. Cao, D. Chen, R. A. Caruso, ACS Appl. Mater. Interfaces **5**, 9421-9428 (2013)

[23] T. Ban, S. Kondoh, Y. Ohya, Y. Takahashi, Phys. Chem. Chem. Phys. **1**, 5745-5752 (1999)

[24] G. D. Lee, S. K. Jung, Y. J. Jeong, J. H. Park, K. T. Lim, B. H. Ahn, S. S. Hong, Appl. Catal. A **239**, 197-208 (2003)

[25] Z. Ren, E. Kim, S. W. Pattinson, K. S. Subrahmanyam, C. N. R. Rao, A. K. Cheetham, D. Eder, Chem. Sci. **3**, 209-216 (2012)

[26] L. Tosheva, V. Valtchev, J. Sterte, Micropor. Mesopor. Mater. **35-36**, 621-629 (2000)

[27] L. Tosheva, B. Mihailova, V. Valtchev, J. Sterte, Micropor. Mesopor. Mater. **48**, 31-37 (2001)

[28] L. Tosheva, J. Sterte, Stud. Surf. Sci. Catal. **142**, 183-190 (2002)

[29] K. Lin, O. I. Lebedev, G. Van Tendeloo, P. A. Jacobs, P. P. Pescarmona, Chem. Eur. J. **16**, 13509-13518 (2010)

[30] S. Zhang, Y. Jiang, S. Li, X. Xu, K. Lin, Appl. Catal. A **490**, 57-64 (2015)

[31] D. Cani, P. P. Pescarmona, J. Catal. **311**, 404-411 (2014)

[32] G. Zhang, J. Sterte, B. J. Schoeman, Chem. Mater. **9**, 210-217 (1997)

[33] L. Tosheva, B. Mihailova, V. Valtchev, J. Sterte, Micropor. Mesopor. Mater. **39**, 91-101 (2000)

[34] A. J. H. P. van der Pol, J. H. C. van Hooff, Appl. Catal. A **92**, 93-111 (1992)

[35] G. Bellussi, A. Carati, M. G. Clerici, G. Maddinelli, R. Millini, J. Catal. **133**, 220-230 (1992)

[36] O. Yazdani, M. Irandoust, J. B. Ghasemi, Sh. Hooshmand, Dyes Pigments **92**, 1031-1041 (2012)

[37] A. Houas, H. Lachheb, M. Ksibi, E. Elaloui, C. Guillard, J.-M. Herrmann, Appl. Catal. B **31**, 145-157 (2001)

[38] N. S. Allen, M. Edge, A. Ortega, G. Sandoval, C. M. Liauw, J. Verran, J. Stratton, R. B. McIntyre, Polym. Degrad. Stabil. **85**, 927-946 (2004)

Figure captions

Figure 1. Fig. 1 XRD patterns of TS-1 beads with different Ti content and the reference silicalite-1.

Figure 2. SEM images of: (a) the resin template, (b) TS-1(0.25), (c) TS-1(0.5) and (d) TS-1(1.0).

Figure 3. SEM images of the surface of: (a) TS-1(0.25), (b) TS-1(0.5) and (c, d) TS-1(1.0) beads.

Figure 4. (a) Nitrogen adsorption isotherms at -196 °C (closed symbols, adsorption; open symbols, desorption) and (b) corresponding BJH desorption pore size distributions of the TS-1 beads.

Figure 5. Raman spectra of TS-1 beads and S-1 and CristalACTiV™ PC500 (anatase) reference samples. The spectra are vertically offset for clarity. The dashed line marks the Raman peak near 960 cm^{-1}, indicative of Ti substitution for Si in the MFI framework.

Figure 6. Pseudo-first-order kinetic plots for the degradation of MB in the absence of a catalyst and in the presence of CristalACTiV™ PC500 or TS-1 beads. The results for the different TS-1 samples are similar.

Figure 7. Attenuation of power stored in microwave cavity with irradiation for 1800 s followed by switching off the light source for CristalACTiV™ PC500 and TS-1(0.25).

Figure 1

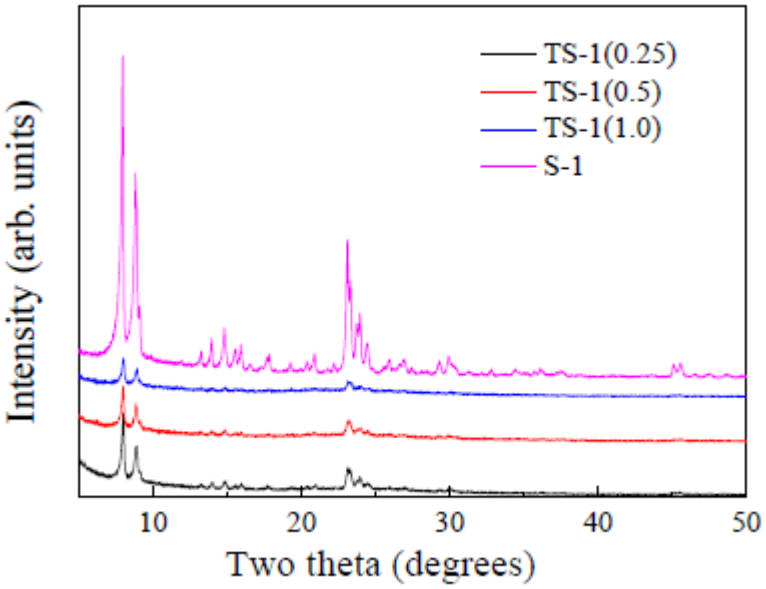
TS-1(0.25)
TS-1(0.5)
TS-1(1.0)
S-1
Intensity (arb. units)
10
20
30
40
50
Two theta (degrees)

Figure 2

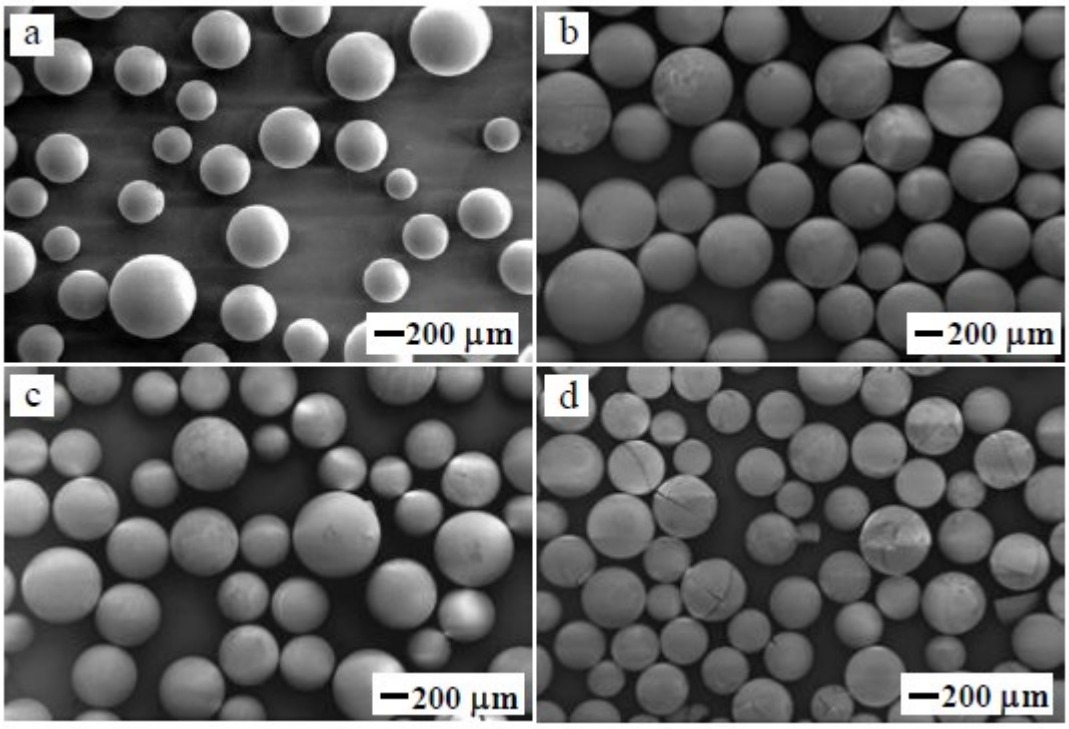

Figure 3

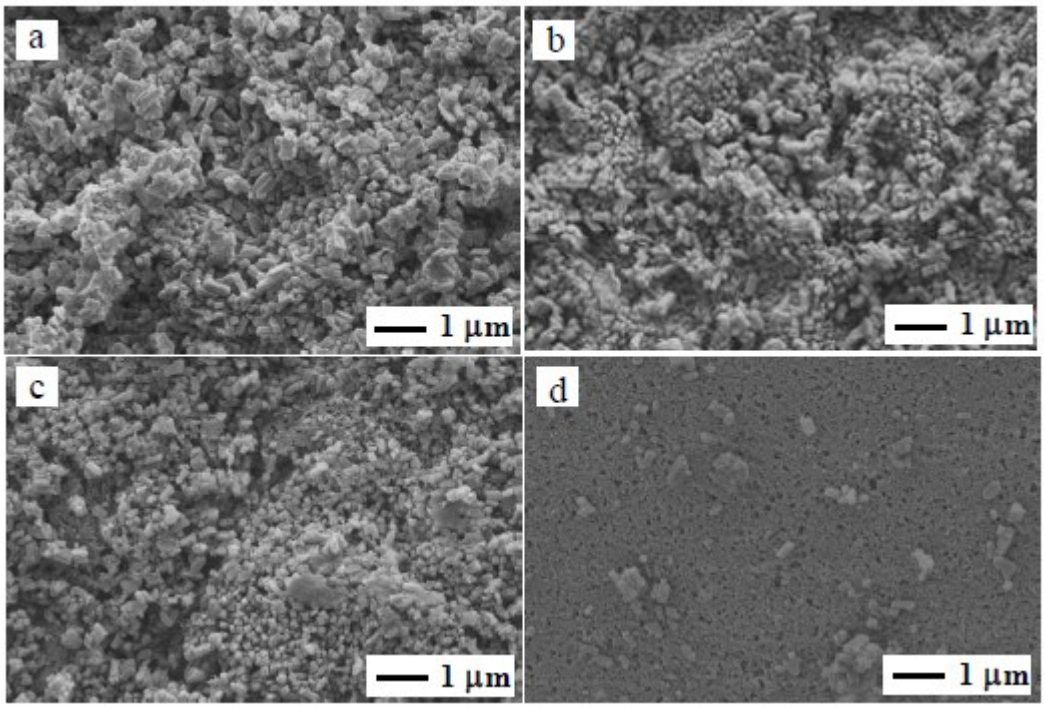

Figure 4

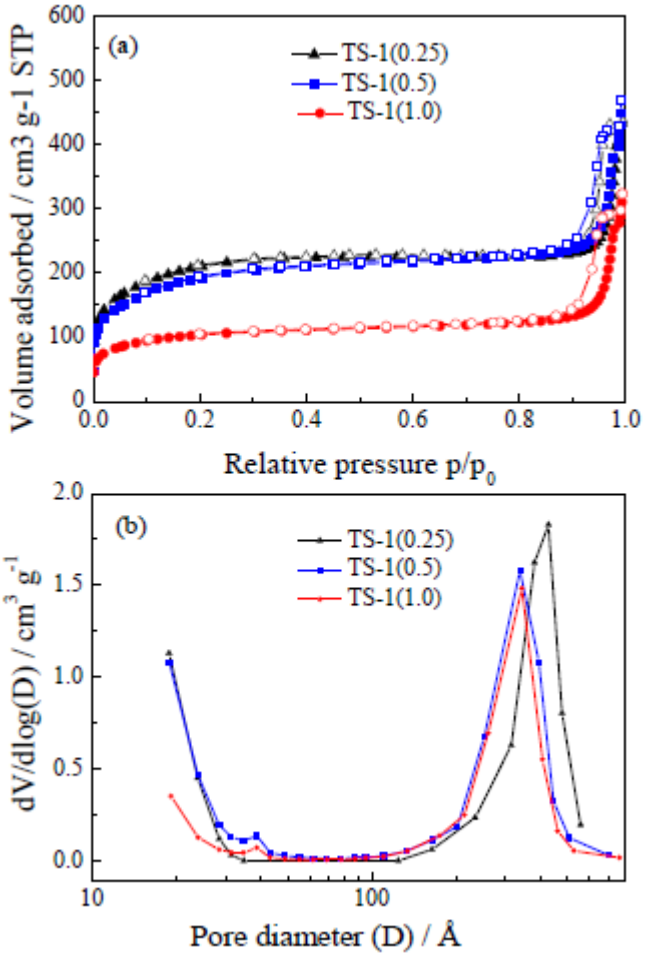
(a)
TS-1(0.25)
TS-1(0.5)
TS-1(1.0)
Volume adsorbed / cm3 g-1 STP
Relative pressure p/p0
(b)
TS-1(0.25)
TS-1(0.5)
TS-1(1.0)
dV/dlog(D) / cm3 g-1
Pore diameter (D) / Å

Figure 5

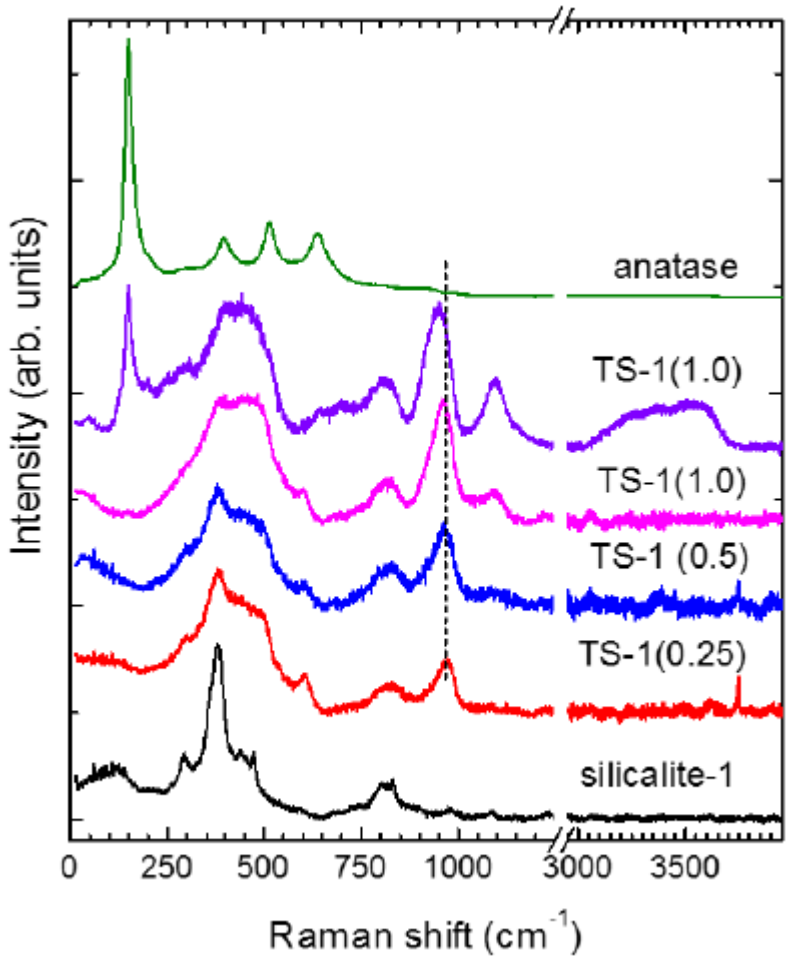
Intensity (arb. units)
anatase
TS-1(1.0)
TS-1(1.0)
TS-1 (0.5)
TS-1(0.25)
silicalite-1
0
250
500
750
1000
3000
3500
Raman shift (cm-1)

Figure 6

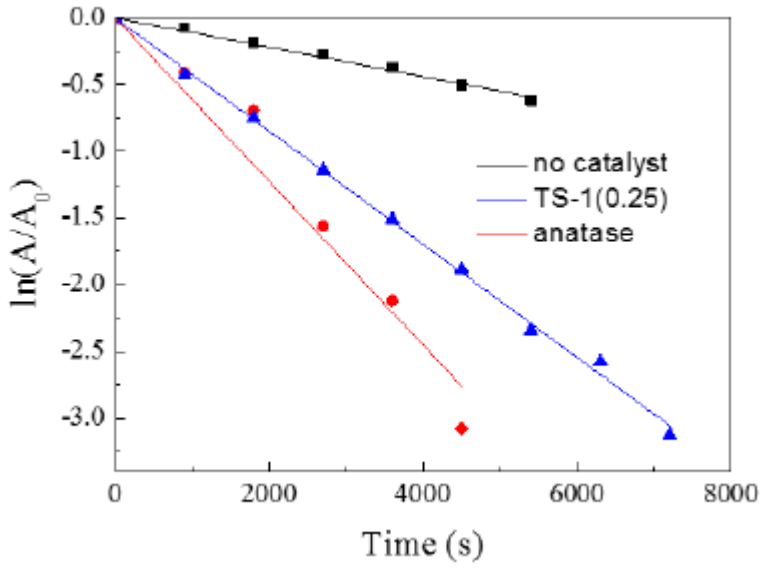
0.0
-0.5
-1.0
-1.5
-2.0
-2.5
-3.0
ln(A/A0)
0
2000
4000
6000
8000
Time (s)
no catalyst
TS-1(0.25)
anatase

Figure 7

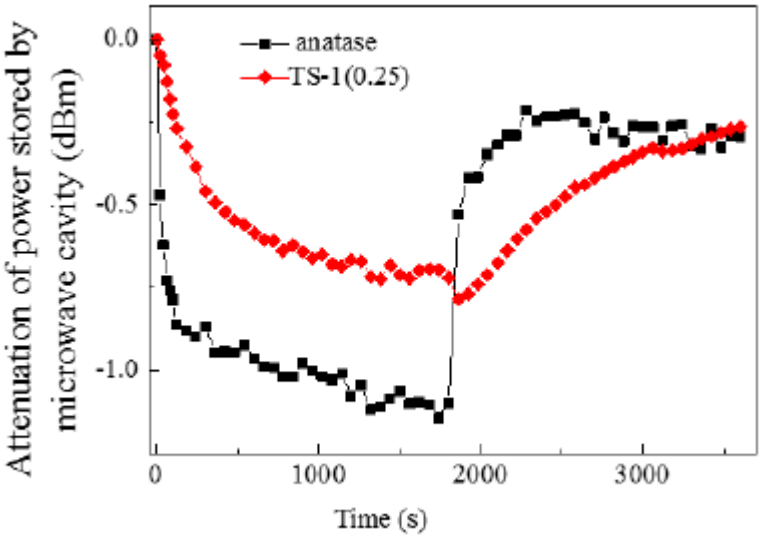
anatase
TS-1(0.25)
Attenuation of power stored by microwave cavity (dBm)
0.0
-0.5
-1.0
0
1000
2000
3000
Time (s)

Table 1. Ti content and nitrogen adsorption data of the TS-1 beads.

Sample	Ti content (wt.%)	S_{BET} ($m^2\ g^{-1}$)	V_{μ} ($cm^3\ g^{-1}$)	V_{total} ($cm^3\ g^{-1}$)	V_{meso} ($cm^3\ g^{-1}$)	S_{EXT} ($m^2\ g^{-1}$)
TS-1(0.25)	1.1	725	0.10	0.67	0.57	506
TS-1(0.5)	3.1	671	0.07	0.73	0.66	508
TS-1(1.0)	6.9	352	0.07	0.50	0.43	196

Table 2. Apparent first order MB degradation rate constants at 35 °C and corresponding correlation coefficients in the presence of TS-1 beads in five consecutive runs.

	k_{app} (s^{-1}) (R^2)[a]		
	TS-1(0.25)	TS-1(0.5)	TS-1(1.0)
Run 1	0.000424 (0.998)	0.000460 (0.953)	0.000455 (0.997)
Run 2	0.000492 (0.991)	0.000516 (0.989)	0.000501 (0.983)
Run 3	0.000480 (0.998)	0.000446 (0.997)	0.000412 (0.998)
Run 4	0.000481 (0.995)	0.000496 (0.995)	0.000463 (0.996)
Run 5	0.000511 (0.987)	0.000495 (0.985)	0.000472 (0.947)

[a] Corresponding values (Run 1) in the absence of catalyst and in the presence of CristalACTiV™ PC500 are 0.000110 (0.991) and 0.000613 (0.954).